Z. Phys. A - Atoms and Nuclei 304, 31-40 (1982)

Zeitschrift für Physik A Atoms and Nuclei

© Springer-Verlag 1982

Angle- and Spin-Resolved Photoelectron Spectroscopy of the Hg $5d^{10}$ Subshell

G. Schönhense, F. Schäfers, U. Heinzmann, and J. Kessler*
Fritz-Haber-Institut der Max-Planck-Gesellschaft, Berlin, Germany
* Physikalisches Institut der Universität Münster,
Synchrotron der Universität Bonn, Federal Republic of Germany

Received September 7, 1981; revised version October 5, 1981

Parameters describing electron spin polarization in Hg $5d^{10}$ subshell photoionization have been measured at rare-gas resonance wavelengths between 73.59 nm and 30.38 nm. The spin parameters as well as asymmetry parameters β of a recent measurement are discussed in comparison with both nonrelativistic and relativistic ab initio calculations of several authors. The importance of many-electron correlations and spin-orbit coupling effects is considered.

1. Introduction

Much experimental work in recent years has clearly demonstrated that photoelectron angular-distribution and spin-polarization measurements provide a very sensitive test of theories in the field of photoionization of atoms. It has turned out that in some cases only the most sophisticated theoretical models are capable of explaining the experimental findings quantitatively over a spectral range of some ten eV. Particularly the many-electron interactions within the subshell under investigation or between electrons of different subshells proved to be of great importance in describing the parameters which govern the photoionization dynamics.

In this paper new experimental results of photoelectron spin polarization parameters for the ionization of the Hg $5d^{10}$ subshell are presented. Angle-resolved measurements have been made using unpolarized resonance VUV radiation from rare-gas discharge lamps in the photon energy range between 16.85 and 40.81 eV. For angle-integrated spin-polarization measurements we utilized circularly polarized synchrotron radiation of four wavelengths between 74 and 58 nm (16.8 and 21.4 eV, respectively) corresponding to the resonance lines mentioned above. The discussion of experimental data includes recent results for the asymmetry parameter β.

The mercury $5d^{10}$ subshell was chosen because relativistic (spin-orbit) effects should play an important role in such a heavy atom ($Z=80$). On the other hand, $5d^{10}$ is an "inner" subshell (below the outermost $6s^2$ subshell) and, in addition to the relativistic effects, many-electron correlations might be of importance.

It is the purpose of this paper to give a detailed description of the apparatus designed for the angle-resolved experiments and to compare the experimental data with calculations of several authors. The comparison is made with a view to learning the relative importance of relativistic and correlation effects.

The first prediction of the general behavior of the asymmetry parameter β in photoionization of d-subshells was made by Manson [1, 2] from a nonrelativistic central-potential model calculation using the Cooper-Zare [3] formula. The relativistic treatment for the Hg $5d^{10}$ subshell was carried out by Walker et al. [4] and Walker and Waber [5]. These authors could explain the deviation of the branching ratio (ratio of the partial cross sections for the $d_{5/2}$ and $d_{3/2}$ subshell) from the statistical ratio 1.5 as being due to the slope of the total cross section as function of the photon energy. Their quantiative calculations in the relativistic central-potential model also show that spin-orbit coupling modifies the nonrelativistic picture insofar as the photoelectrons ejected from the subshells with $j=l\pm 1/2$ have, in general, slightly different angular distributions.

One obvious reason for this is that the photoelectrons ejected by photons of a given energy from the $d_{5/2}$ or $d_{3/2}$ subshells have different kinetic energies,

0340-2193/82/0304/0031/$02.00

owing to the fine-structure splitting between the final ionic states $^2D_{5/2}$ and $^2D_{3/2}$.

In a similar relativistic model, also using the Slater approximation for the exchange interaction (DS), Kim et al. [6] and Keller and Combet Farnoux [7] have calculated the photoelectron angular distribution for Hg $5d^{10}$ yielding parameters which are quantiatively different from the results of Walker and Waber [5]. Recently, Dirac-Fock calculations performed by Tambe et al. [8, 9] have shown good quantitative agreement with measurements of the branching ratio (see below).

All theoretical results mentioned above have been obtained in the single-electron model, i.e. without taking many-electron correlations into account. Ivanov et al. [10] have calculated β in the non-relativistic Random-Phase Approximation with Exchange (RPAE). In this calculation many-body interactions between the electrons in the $5d^{10}$ subshell are included. At the time the present measurements were carried out, no calculation of the photoelectron polarization was available. Later Cherepkov [11] calculated the spin parameter ξ using the matrix elements of [10]. Very recently a Relativistic Random-Phase Approximation (RRPA) calculation was made by Johnson et al. [12] which accounts for electron correlations as well as for relativistic (spin-orbit) effects.

Most of the experimental work concerning Hg photoionization has been concentrated on total and partial cross sections. Photoabsorption of Hg vapor has been studied earlier by Beutler [13], and later by Berkowitz and Lifshitz [14] and Lincke and Stredele [15]. Photoionization cross sections were measured by Brehm [16], Cairns et al. [17], Dehmer and Berkowitz [18] and Süzer et al. [19]. The branching ratio of the $5d_{5/2}$ and $5d_{3/2}$ subshell cross sections has been investigated by Walker et al. [4], Dehmer and Berkowitz [18], Süzer et al. [19], Svensson et al. [20], Nilsson et al. [21], and more recently by Shannon and Codling [22] using synchrotron radiation.

The photoelectron angular distribution has been measured for the Hg $6s^2$ valence shell by Brehm and Höfler [23], for the Hg $5d^{10}$ subshell by Harrison [24], Niehaus and Ruf [25] and recently by Schönhense [26]. The angle-integrated spin polarization for photoionization using circularly polarized light has been measured by Schäfers et al. [27] in the autoionization region above the first ionization threshold ($h\nu = 10.43$ eV).

The angular dependence of the photoelectron polarization for the case of ionization of unpolarized atoms with unpolarized light for dipole transitions is given by the expression [28, 29]

$$\mathbf{P}(\theta) = \frac{2\xi \cos\theta [\hat{k}_i x \hat{k}_0]}{1 - \frac{\beta}{2} \cdot P_2(\cos\theta)}. \tag{1}$$

The unit vectors $\hat{k}_i$ and $\hat{k}_0$ (forming the angle θ) are directed along the momenta of the incoming photon and the outgoing electron, respectively. $P_2(\cos\theta) = \frac{3}{2} \cdot \cos^2\theta - \frac{1}{2}$ is the second Legendre polynomial. In the definition of the energy-dependent spin parameter ξ we follow that of Lee [29]. The polarization vector is oriented normal to the reaction plane in analogy to the electron spin polarization produced by scattering of unpolarized electrons on unpolarized atoms [30].

A common feature of spin polarization formulae is that the denominator is proportional to the total number of electrons produced, i.e. in this case to the differential cross section [3]:

$$\frac{d\sigma}{d\Omega}(\theta) = \frac{Q}{4\pi}\left[1 - \frac{\beta}{2} P_2(\cos\theta)\right]. \tag{2}$$

Here Q is the total cross section and the asymmetry parameter β describes the deviation of the photoelectron angular distribution from isotropy.

2. Experimental Arrangement and Method

The present investigation of the photoelectron polarization normal to the reaction plane (spanned by the incoming photon beam and the direction of observation) was carried out using the set-up depicted in Fig. 1. The horizontal cut through the reaction plane of the photoionization process and through the scattering plane of the Mott detector shows the VUV light sources, the photoelectron spectrometer, and (in another scale) the accelerator and Mott-scattering chamber for spin polarization analysis. The vacuum chamber containing the lamps is pumped by an oil diffusion pump; the mercury beam is frozen by means of a large liquid-nitrogen cool trap (surface area 2,500 cm^2) which was placed approximately 20 cm above the atomic-beam nozzle. The cool trap reduced the mercury background pressure during the measurement to less than 10^{-6} mbar with operating atomic beam. The Mott-scattering chamber was pumped via the accelerator tube to about $4 \cdot 10^{-5}$ mbar which is sufficiently low for high-energy Mott-scattering.

2.1. Light Sources and Photoelectron Spectrometer

A description of the VUV light sources has been given elsewhere [31] so that only the main charac-

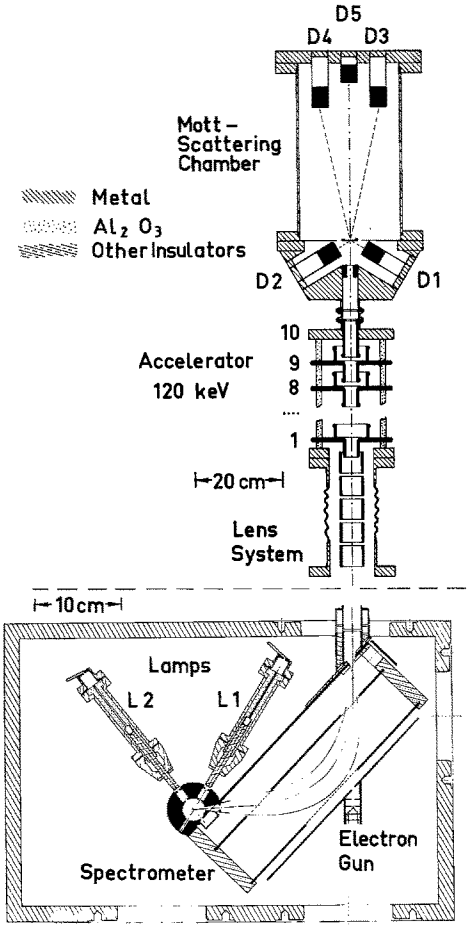

Fig. 1. Semi-schematic horizontal section of the apparatus

teristics need to be reported here: A cold-cathode *dc* discharge (up to 200 mA) is maintained in an Al_2O_3 capillary (2 mm i.d., 60 mm length) between the water-cooled cathode (Copper-Cobalt-Beryllium alloy) and the anode, which is inserted into the Al_2O_2 capillary. The discharge tubes and particularly the inlet system for the gas supply are bakable in order to remove impurities like oil and water from the discharge region. Such impurities can reduce the light intensity of certain resonance wavelengths by more than one order of magnitude. The lamps are differentially pumped by means of a mechanical pump ($20\,m^3h^{-1}$) via a liquid nitrogen cooled Zeolite trap. Without passing through a window the resonance radiation produced in the Helium or Neon discharge emerges into the high-vacuum chamber and enters the ionization chamber through a system of apertures which confines the diameter of the light beam to 2.5 mm. The photon flux through these apertures is nearly $10^{13}\,s^{-1}$ for the strongest HeI and NeI line and approximately one order of magnitude less for the strongest HeII and NeII line under optimum discharge conditions.

In the center of the ionization chamber (copper hollow cylinder) the radiation intersects an Hg atomic beam directed perpendicular to the drawing plane. The target atoms expand from an overheated nozzle (ending 5 mm below the photon beams) which is connected to a Hg reservoir. Furnace and nozzle are heated by means of a temperature-controlled stream of hot air. Since all parts of the oven are made from non-magnetic material (essentially copper and titanium) this technique creates no disturbing magnetic fields in the target region. Details of the device [32] will be given elsewhere.

The electron spectrometer [33] is a cylindrical mirror analyzer designed following the parameters of Risley [34].

Outer cylinder 90 mm radius.

Inner cylinder 35 mm radius.

Slit-to-slit distance 246 mm.

Angle of entrance 43.2°.

Its virtual entrance aperture is the photo target itself (approximate size 2.5 mm), the exit slit could be varied between 1 and 3 mm. The energy resolution was less than 30 meV FWHM for pass energies below 3 eV. Fringe field corrections are made by means of thin layers of colloidal graphite on Mykroy insulators.

2.2. *Accelerator and Mott-Scattering Analyzer*

An electrostatic five-element zoom lens with four pairs of deflection plates focuses those photoelectrons which have passed the exit slit of the spectrometer into the entrance of an accelerator. In the ten-element acceleration tube with parabolic increase of the potential the electrons are accelerated to 120 keV and then are scattered on a thin gold foil ($180\,\mu g\,cm^{-2}$). The number of electrons scattered into the angular interval $120° \pm 25°$ and $-120° \pm 25°$ is detected by the surface barrier detectors $D1$ and $D2$ (Ortec CA 018-300-100). The scattering asymmetry appearing in this spin-dependent (Mott-)scattering process allows the determination of the spin-polarization component normal to the scattering plane [35] which is identical to the drawing plane of Fig. 1.

The asymmetry function (Sherman function) for this arrangement has been found [36] to be $S = -0.26 \pm 0.01$. The uncertainty of S limits the accuracy of the polarization measurements to 4% (relative accuracy). The detectors $D3$ and $D4$ mounted under 13° in the forward direction are monitors for the local stability of the electron beam, because the Sherman function is very small there, $S(13°, 120\,keV) = 0.002$. For weak signals the primary electron beam

could be detected using $D5$. A simple electron gun is mounted on the rear of the electron spectrometer so that its beam passes through the exit slit under the same angle as the photoelectrons analyzed. This electron beam allows adjustment of the voltages of the electron optics with a fluorescent-screen monitor in the position of the gold foil. It also serves as a $P=0$ standard when adjusting the Mott detector.

2.3. Measurement of the Spin Parameter ξ

For the determination of the parameter ξ the favorable angle between photon and electron momentum is the "magic" angle $\theta_m = 54°44'$, defined by $P_2(\cos\theta_m)=0$. At this angle the denominator of the polarization formula (1) equals 1 so that the asymmetry parameter β has no influence on the photoelectron polarization measured. This is in complete analogy to angularly resolved measurements of the total photoionization cross section. The electron spectrometer accepts photoelectrons ejected into the interval $\theta=\theta_m\pm5.5°$ with respect to the axis of lamp $L2$ and $\theta=\pi-\theta_m\pm5.5°$ with respect to $L1$. The correction of the experimental data due to the solid angle interval accepted by the electron spectrometer turned out to be negligible. Thus (1) yields:

$$P(\theta_m)=2\xi\sin\theta_m\cos\theta_m=0.94\xi. \tag{3}$$

Apparatus-related asymmetries of the Mott analyzer have been eliminated by alternating operation of $L1$ and $L2$ with counting periods of 60 s. When switching from one lamp to the other the spin polarization vector reverses its sign, because from (1) one has $P(\theta_m)=-P(\pi-\theta_m)$. In order to measure the background count rate with a lamp running, the photoelectron spectrometer was tuned to such a pass energy that only background electrons could pass the exit slit. Switching over the power supply of the lamps as well as tuning the electron spectrometer was facilitated by a small microprocessor which also collected the true and the background counts and calculated the degrees of spin polarization. Thus, the cycle of the measuring procedure (60 s signal ($L1$), 60 s signal ($L2$), 60 s background) was fully automatized.

The degree of spin polarization was calculated from the following equation:

$$P=S^{-1}\frac{\sqrt{N_{D1,L1}N_{D2,L2}}-\sqrt{N_{D1,L2}N_{D2,L1}}}{\sqrt{N_{D1,L1}N_{D2,L2}}+\sqrt{N_{D1,L2}N_{D2,L1}}} \tag{4}$$

where for each counting interval $N_{Di,Lj}$ is the number of signals in the detector Di (after subtraction of the background) with lamp Lj operating. Due to the negative sign of S the parameter ξ is positive, if $D2$ shows the higher count rate during operation of $L1$ and the lower count rate during operation of $L2$. The single statistical error of P is

$$\Delta P=S^{-1}(1-(SP)^2)\tfrac{1}{4}\left(\sum_{i=1}^{4}\frac{1+2U_i/N_i}{N_i}\right)^{1/2} \tag{5}$$

where N_i is one of the four numbers mentioned in (4) and U_i is the corresponding number of background counts in the same channel. The counts of many 60 s intervals were added accordingly.

2.4. Sources of Error and Test Measurements

In addition to the statistical error (5) and the uncertainty in S (both known numerically) there are some other sources of error. The following have been investigated:

a) The trajectories of the photoelectrons must not be distorted by fields in the target region. The most probable cause of electric fields is that the atomic-beam nozzle has a different potential than the inner walls of the ionization chamber. If this occurs not all photoelectrons produced start from the same electric potential, i.e. the zero of the energy is poorly defined. This manifests itself in a deteriorated energy resolution, visible in the photoelectron spectra. Such potential differences have been compensated in test measurements by applying a small correction voltage between the nozzle and the ionization chamber. The voltage was determined empirically by minimizing the peak widths in the photoelectron spectra. The magnetic field in the target region was reduced to 1 % of the earth's magnetic field by three pairs of Helmholtz coils. The influence of this remnant field on electron trajectories and spin was negligible.

b) Angular distribution and spin must not be influenced by scattering of the ejected photoelectrons on target atoms. This source of error occurs at high target densities and corresponds to the influence of multiple scattering on angular distribution and polarization in low-energy electron scattering, a phenomenon which has been studied in detail by Eitel et al. [37] for the Hg target. Scattering processes always lowered the asymmetry parameter β and the spin parameter ξ (tendency to isotropic angular distributions) in agreement with the results for multiple scattering [37]. Test measurements showed that for the data reported in this paper no pressure dependence could be observed when the density of the atomic beam was approximately 10^{10} atoms mm^{-3}. This density value has been estimated using the Hg mass throughput and the approximate size of the

atomic beam in the target region. Only during the measurements in the autoionization range [27] has a pressure dependence of the degree of spin polarization been observed even at lower densities. The reason for this behavior is the large scattering cross section [38] at very small electron energies.

c) Sources of error connected with the Mott-scattering analyzer and the necessary precautions have been discussed in detail by Jost and Kessler [35]. Finally it should be noted that the microprocessor was able to exclude from the evaluation those data which had been falsified due to pulses in the counting electronics caused by microdischarges in the 120 kV high-voltage region.

3. Results for the Spin Parameter ξ and Discussion

The spin parameter ξ has been measured at the following resonance wavelengths [39]:

NeI, 73.59 nm
HeI, 58.43 mm and 53.70 nm
NeII, 46.16 ± 0.09 nm, 44.64 ± 0.14 nm, 40.65 ± 0.06 nm
HeII, 30.38 nm.

In the case of NeII the resonance radiation consists of unresolved groups of closely adjacent lines within the wavelength intervals given by the error bars. The parameters ξ measured are shown in Figs. 2 and 3. Figure 2 shows the results for the $d_{3/2}$ spin-orbit subshell, i.e. the Hg^+ ion is left in the $^2D_{3/2}$ final state. Throughout this paper, experimental data for

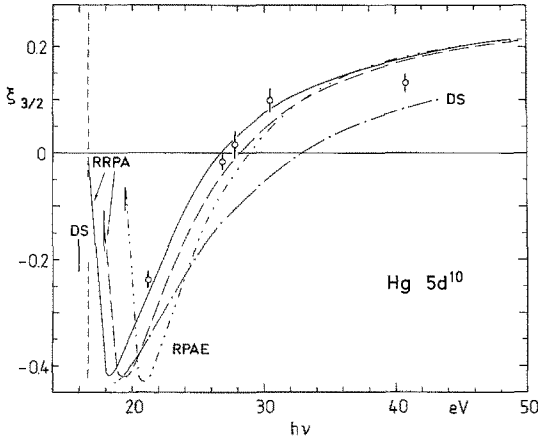

Fig. 2. Spin parameter ξ versus photon energy $h\nu$ for photoelectrons from the mercury $5d^{10}$ subshell, leaving a $Hg^+ {}^2D_{3/2}$ ion. The dashed vertical line gives the experimental threshold. Theoretical calculations: -·-·-· Dirac-Slater, calculated using matrix elements of Keller and Combet Farnoux [7]. -··-·· RPAE, Ivanov et al. [10], Cherepkov [11]. ---- RRPA with theoretical thresholds, Johnson et al. [12]. ——— RRPA with experimental thresholds, Johnson et al. [12]

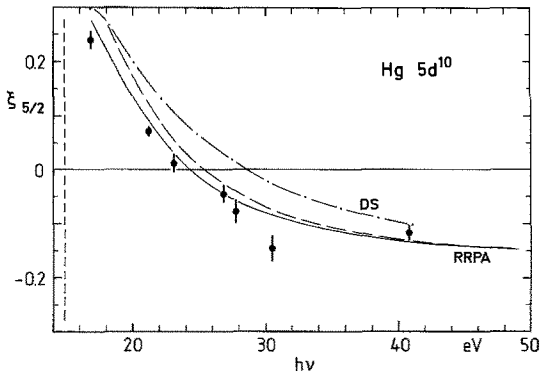

Fig. 3. The same as Fig. 2 but for a residual ion in the $Hg^+ {}^2D_{5/2}$ state

the $d_{3/2}$ subshell are plotted as open symbols, whereas full symbols correspond to the $d_{5/2}$ subshell (Fig. 3). The error bars of the data points represent one standard deviation. The vertical dashed line on the left side of each Figure is the experimental photoionization threshold of the corresponding subshell [40].

Four results of theoretical ab initio calculations are also shown in Fig. 2. The Dirac-Slater (DS) curves have been calculated using radial dipole matrix elements and phase-shift differences of Keller and Combet Farnoux [7] together with Lee's [29] expression for the spin parameter ξ. The matrix elements used are the results of a relativistic central-potential calculation in the single-electron model [7], i.e. in the *jj*-coupling scheme.

The calculation in Relativistic Random-Phase Approximation (RRPA) was made by Johnson et al. [12]. In this theory account is taken of the spin-orbit interaction and of electron-electron correlations including coupling between the various photoionization channels. These final-state coupling effects induce the intermediate-coupling scheme (multichannel intermediate-coupling approximation), which should be more appropriate for Hg than pure *jj* or LS coupling. All RRPA curves cited in this paper result from a calculation that considers excitations of the $5d$ and $6s$ electrons (eight-channel calculation).

The dashed curve is based on theoretical (Dirac-Fock) thresholds, marked in Fig. 2 by the short vertical line on the left side of the curve, whereas in the calculation of the full curve, the DF thresholds had been replaced by experimental ionization potentials [40].

The result in non-relativistic Random-Phase Approximation with Exchange (RPAE) only for $d_{3/2}$ has been obtained by Cherepkov [11] employing matrix elements and phase-shift differences of Ivanov et al. [10]. In this context the expression "non-

relativistic" means that the spin-orbit interaction in the continuum states is neglected (*LS* coupling). Nevertheless, such a theoretical model is applicable to photoelectron spin-polarization calculations [28, 41]. In the RPAE many-electron interactions within the $5d^{10}$ subshell (intrashell correlations) have been taken into account. Both RPA theories include energy-dependent exchange interaction.

All calculated curves reflect the same general behavior which is verified by the measurements. Quantitatively the RRPA curve using experimental thresholds shows the best agreement with the experiment, though the agreement seems to be not as good as it is in the valence-shell photoionization of the rare gases studied recently [42, 43]. A probable reason is that more intershell correlations have to be taken into account. Being an "inner" subshell, the $5d^{10}$ shell is exposed to the many-electron influences of its outer and inner neighboring shells. The main reason for the deviations of the other theoretical curves from the measured points lies in the theoretical threshold positions (short vertical lines). Since, as a consequence of the energy dependence of the Coulomb scattering phase shift, ξ varies rapidly just above threshold, the small energy shifts of the curves cause large differences in the parameter ξ. The slope of the DS curve is too small as compared with experiment; this must be attributed to the neglect of many-electron correlations. It can be shown that particularly interchannel correlations between the εf and εp continuum waves reached by the dipole transition are responsible for the disagreement [32].

In the comparison of the experimental results with theories no effects of autoionization are considered. Over the photon-energy range investigated there exist, however, autoionizing states due to simultaneous excitation of two electrons. None of the theories mentioned takes into account double excitations but such features have been observed in the Hg I absorption spectrum [44]. The resonances should also be present in the dynamical parameters discussed in the present work; since the energetic positions and the widths are known only approximately, a possible influence of double-excitation autoionizing states on the measurements cannot be completely excluded. For a quantitative estimation of these resonance effects more experimental data, particularly detailed cross section measurements, are highly desirable.

The RPAE applies the pure *LS*-coupling scheme in which the branching ratio of the partial cross sections $Q_{5/2}:Q_{3/2}$ has its statistical value, for *d* electrons 1.5. The polarization of photoelectrons from unpolarized atoms arises due to spin-orbit interaction. If the fine-structure splitting is not resolved, the polarization effect vanishes in the non-relativistic model [28]. In the mean value of the spin parameters of the two spin-orbit components, $\xi_{3/2}$ and $\xi_{5/2}$ are to be weighted with the corresponding partial cross sections, thus yielding:

$$\bar{\xi}=\frac{\xi_{3/2}+\frac{Q_{5/2}}{Q_{3/2}}\cdot\xi_{5/2}}{1+\frac{Q_{5/2}}{Q_{3/2}}}. \tag{6}$$

Consequently, in the non-relativistic approximation the sign of the spin-polarization must be opposite for the two spin-orbit components and the ratio of the spin parameters $\xi_{5/2}:\xi_{3/2}$ equals $1:(-1.5)$. Obviously this relation is not fulfilled for every photon energy. For example at $h\nu=21.22\,\mathrm{eV}$ one finds $\xi_{3/2}:\xi_{5/2}=-3.3\pm0.5$, a value whose modulus is even larger than the branching ratio of 2.3 ± 0.2 measured at 21.2 eV [22]. From these values it follows that a mean spin-polarization with $\bar{\xi}=-0.03\pm0.01$ remains at this photon energy even if the fine-structure splitting is not resolved.

Walker et al. [4] demonstrate that the deviation of the branching ratio from the statistical value is essentially due to the difference in the kinetic energies of electrons corresponding to the $^2D_{3/2}$ or $^2D_{5/2}$ ionic states. In Fig. 4 the "kinetic-energy effect" is eliminated because the ξ parameter is plotted against E_{kin} instead of $h\nu$. Now the two experimental points corresponding to $h\nu=21.22\,\mathrm{eV}$ appear at energies which differ in 1.86 eV ($E_{\mathrm{kin}}=4.51$ or 6.38 eV). In order to compare the measurements with

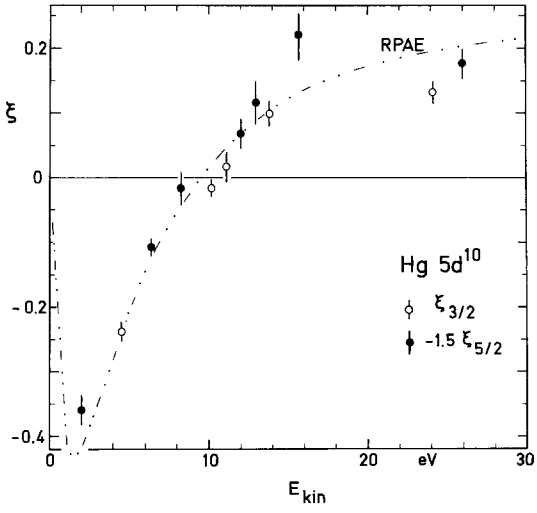

Fig. 4. Experimental results from Figs. 2 and 3 as a function of the kinetic energy E_{kin} of the photoelectrons. For comparison with the non-relativistic RPAE calculation [10, 11] the $\xi_{5/2}$ values from Fig. 3 have been multiplied by -1.5

the non-relativistic theory, the $\xi_{3/2}$ data points have been multiplied by -1.5 (statistical ratio). An important difference between the plots against $h\nu$ or against E_{kin} is that in the latter representation the threshold positions are set equal (at $E_{kin}=0$).
In Fig. 4 the agreement between the RPAE curve and the experimental points is clearly improved as compared with Fig. 2. One can conclude that indeed the main reasons for the disagreement in Fig. 2 are firstly the "kinetic-energy effects" (i.e. spin-orbit coupling in the final ionic states) and secondly the difference between experimental and theoretical ionization energies. The slight difference between the $\xi_{3/2}$ and $-1.5\xi_{3/2}$ values signifies a deviation from the non-relativistic picture caused by spin-orbit interaction.

4. Results for the Spin Parameter $\mathscr{A}$

In photoionization of unpolarized atoms using unpolarized light the photoelectron polarization averaged over all angles of emission vanishes for reasons of symmetry. This, however, does not hold if the photoelectrons produced are ejected by circularly or elliptically polarized light. In this case an average spin polarization remains which is proportional to the degree of circular polarization of the radiation. This process can partly be understood to be a spin-polarization transfer from the photons absorbed onto the photoelectrons produced; it is described by the spin parameter $\mathscr{A}$ [28] which is the ratio of the spin polarization of the electrons and the spin polarization (i.e. degree of circular polarization) of the photons. $\mathscr{A}$ can also be seen as an electron polarization itself in the (ideal) case of the ionization using completely circularly polarized light. But in the experiment, especially in the VUV region, one has in general elliptically polarized radiation only. The measurements of $\mathscr{A}$ at Hg, reported in this section, have been made using elliptically polarized synchrotron radiation of the 2.5 GeV synchrotron in Bonn. A description of the experimental arrangement and technique is given in [27]. In this experiment it was not possible to select photoelectrons of a particular subshell via photoelectron spectroscopy. The reason is that all photoelectrons produced had to be extracted by an electric field, regardless of their direction of emission, which causes a broad energy distribution of the photoelectrons.
The measurement of $\mathscr{A}$ has been made at photon wavelengths between 74 and 58 nm. In this wavelength range photoelectrons are ejected from the Hg $6s$, $5d_{3/2}$ and $5d_{3/2}$ subshells. According to measurements of Shannon and Codling [22] the cross section for ionization in the $5d^{10}$ subshell lies between 8 and 14 Mb, whereas the $6s^2$ cross section does not exceed 0.7 Mb in this spectral range. For this reason the contribution of photoelectrons from the valence shell has been neglected and only the $5d^{10}$ subshell photoionization is considered in the following.
From the theories of Cherepkov [28] and Lee [29] it follows that similar to $\xi_{5/2}$ and $\xi_{3/2}$ also the parameters $\mathscr{A}_{5/2}$ and $\mathscr{A}_{3/2}$ (corresponding to photoelectrons from the $d_{5/2}$ and $d_{3/2}$ spin-orbit subshell, respectively) differ in sign. Thus the measurement yields the mean value of the two parameters, weighted with the corresponding partial cross sections $Q_{5/2}$ and $Q_{3/2}$ (analogously to (6)):

$$\mathscr{A}=\frac{\mathscr{A}_{3/2}+\frac{Q_{5/2}}{Q_{3/2}}\cdot\mathscr{A}_{5/2}}{1+\frac{Q_{5/2}}{Q_{3/2}}}. \tag{7}$$

Figure 5 shows the experimental results as error bars (one standard deviation). For comparison only theoretical results of an RRPA calculation [12] are available which show the same general trend as the measurement. Again, the calculation using experimental thresholds yields results closer to the measurement. The difference between the RRPA and experiment is also visible in the branching ratio $Q_{5/2}/Q_{3/2}$ itself. Measurements [22] show that close to threshold the RRPA [12] overestimates the deviation of $Q_{5/2}/Q_{3/2}$ from the statistical ratio 1.5. The DF calculation of Tambe et al. [8] shows good agreement with the experimental branching ratio but no DF values for $\mathscr{A}$ are available as yet.

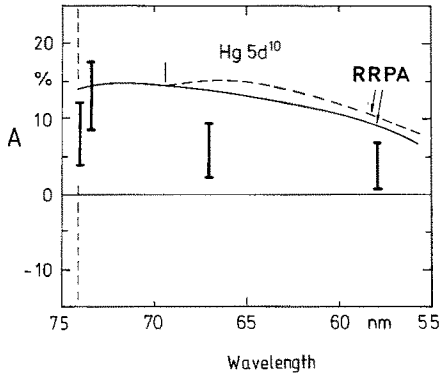

Fig. 5. The spin parameter $\mathscr{A}$ for photoelectrons from the Hg $5d^{10}$ subshell as a function of the photon wavelength. The dashed vertical line is the experimental $d_{3/2}$ threshold. The theoretical RRPA curves have been calculated by Johnson et al. [12]. ---- using theoretical threshold positions, ——— using experimental threshold positions

5. Discussion of Results for the Asymmetry Parameter β

The experimental results for the asymmetry parameter β and the corresponding experimental technique have been reported previously [26]. In the meantime several important theoretical calculations of β have become available so that a discussion of all theoretical data in comparison with measurements seems worthwhile.

Figure 6 shows the variation of β with the kinetic energy of the photoelectrons. Open symbols correspond to the $^2D_{3/2}$ ion, full symbols to the $^2D_{5/2}$ ion. The values measured by Harrison [24] (triangles) and Niehaus and Ruf [25] (squares) agree well with the recent measurements of Schönhense [26] (circles).

In this figure the results of two non-relativistic calculations are plotted. The upper curve has been obtained by Ivanov et al. [10] in the RPAE taking into account correlations within the $5d^{10}$ subshell. The matrix elements and phase shifts of that calculation are identical to those used for the RPAE curve in Figs. 2 and 4. The lower curve has been calculated by Manson [2] in the Hartree-Slater central-potential model (HS) employing Herman-Skillman wavefunctions. Both curves show the behavior of β which is verified by the experiments. Similar to the results for ξ, the correlated calculation gives quantitatively better agreement. It should, however, be mentioned that the discrepancy in the threshold positions which was discussed in Fig. 2 still exists.

Relativistic theories take into account the fine-structure splitting of the final ionic states as well as spin-orbit interaction in the continuum states. As a consequence of spin-orbit coupling the β parameters are different for ions left in the $^2D_{5/2}$ or $^2D_{3/2}$ state (i.e. for ionization of the $d_{5/2}$ or $d_{3/2}$ spin-orbit subshell).

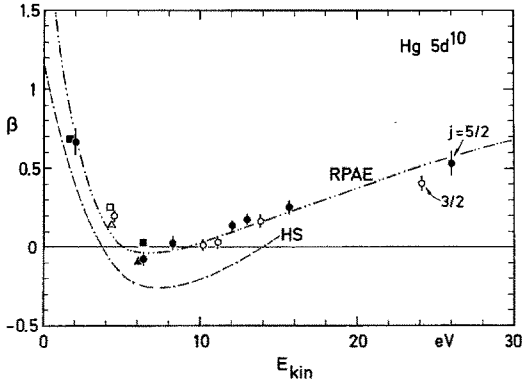

Fig. 6. The asymmetry parameter β for Hg $5d^{10}$ as a function of the kinetic energy E_{kin} of the photoelectrons. Experiments: triangles, Harrison [24]; squares, Niehaus and Ruf [25]; circles, Schönhense [26]. Non-relativistic theories: Hartree-Slater, Manson [2]; RPAE, Ivanov et al. [10]

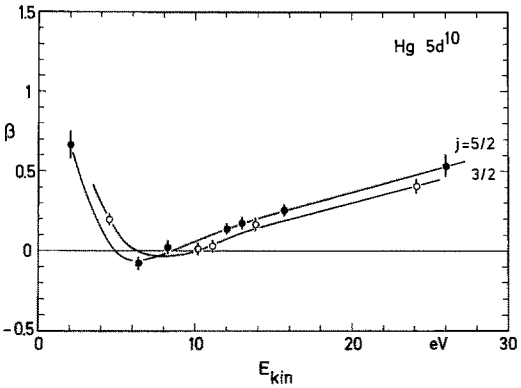

Fig. 7. Tentative curves through the experimental points from Fig. 6

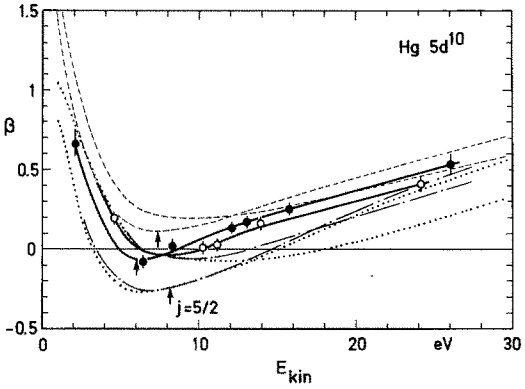

Fig. 8. Comparison of the experimental points and curves from Fig. 7 with relativistic Dirac-Slater calculations. Dashed curves Walker and Waber [5], dotted curves, Kim et al. [6], chain curves, Keller and Combet Farnoux [7]. The arrows denote curves corresponding to $d_{5/2}$

For Hg this difference is observable even if the photoelectrons corresponding to the two different ionic states have the same kinetic energy. This is illustrated in Fig. 7 in which the experimental data points have been connected by tentative curves (without considering autoionization resonances [17, 44]). Analogously to Fig. 4, the "kinetic energy effect" is eliminated because the abcissa is the photoelectron energy.

In Fig. 8 three relativistic central-potential calculations are compared with the experimental points and curves from Fig. 7. In the Dirac-Slater model of Walker and Waber [5], Keller and Combet Farnoux [7] and Kim et al. [6]* no many-electron interactions are taken into account. The theoretical curves show in principle the same behavior as the experiment. Quantitatively, however, deviations exist in the depth and position of the minima as well as in the magnitude of the difference between the two spin-orbit split curves ($j=l\pm1/2$).

* In this calculation not only dipole processes but also higher multipole transitions are included

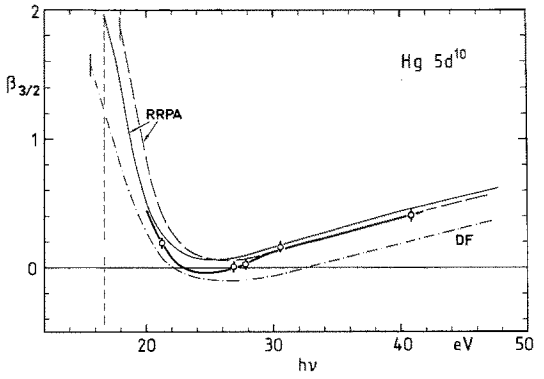

Fig. 9. Comparison of the experimental points (connected by the tentative curve) with a relativistic Dirac-Fock calculation and a RRPA calculation for a residual $^2D_{3/2}$ ion. The abscissa is the photon energy. -·-·-· Dirac-Fock, Tambe et al. [9]. - - - - RRPA with theoretical threshold, Johnson et al. [12]. ——— RRPA with experimental thresholds, Johnson et al. [12]. ——— tentative curve through the experimental points

In Figs. 9 and 10 a relativistic Dirac-Fock calculation [9] and a Relativistic Random Phase Approximation [12] are plotted against photon energy in comparison with the experiment. Some details of the methods of calculation are essential for the discussion. The DF calculation of Tambe et al. [9] employs atomic wavefunctions as initial-state wavefunctions, whereas a completely relaxed ionic core is used to generate the wavefunctions of the final continuum states. Exchange is considered exactly within the framework of single-particle wavefunctions, but neither interchannel coupling nor any other sort of correlation effects are included (pure *jj*-coupling scheme). The RRPA calculation of Johnson et al. [12] also starts from single-particle DF calculations but adds many-electron correlations within the $5d^{10}$ and $6s^2$ subshells including interchannel coupling of the various photoionization channels (multichannel intermediate-coupling approximation). The effects of core relaxation [45], however, are not included.

The experimental tentative curves in Figs. 9 and 10 are very close to the RRPA results. As in Figs. 2 and 3, the curves based upon experimental thresholds show better agreement with the experiment than those calculated using theoretical thresholds. Only in the region around the minimum of the curves, a small difference between RRPA theory and experiment appears. Here the experimental tentative curve lies between the RRPA and the DF curves.

The comparison shows that electron-electron correlations change the single-electron DF result significantly and bring theory and experiment in good quantitative agreement. The small discrepancies which remain may be due to the neglect of correlations with subshells more tightly bound or effects of core relaxation.

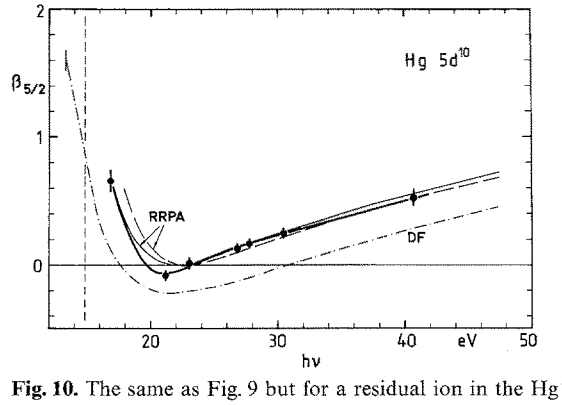

Fig. 10. The same as Fig. 9 but for a residual ion in the $Hg^+ {}^2D_{5/2}$ state

6. Conclusions

In this paper experimental values of three different photoionization parameters are compared with ab initio calculations obtained in various theoretical approximations. For the *d*-subshell photoionization studied even a non-relativistic central-potential calculation qualitatively reveals the right behavior. Relativistic and many-electron correlation effects manifest themselves in modifications of the quantitative shapes of the curves.

The essential consequence of the relativistic spin-orbit interaction is the energetic fine-structure splitting of 1.86 eV between the final ionic states $^2D_{3/2}$ and $^2D_{5/2}$. This energetic spin-orbit splitting induces the so called "kinetic-energy effect" in the dynamical parameters measured which can be eliminated by considering the parameters as functions of the photoelectron kinetic energy instead of the photon energy. In this case only a relatively small deviation of the non-relativistic picture remains, visible in the deviations of the parameters $\xi_{3/2}$ and $-1.5\xi_{5/2}$ from one smooth curve in Fig. 4, and also in the small splitting between the asymmetry parameters $\beta_{3/2}$ and $\beta_{5/2}$ in Fig. 7. This experimental result agrees with the deduction of Niehaus and Ruf [25] and confirms the general theoretical prediction of Walker and Waber [5].

In this context it is worth pointing out that the situation in *s*-subshell photoionization [27] is very different. There is no spin-orbit coupling and consequently no "kinetic-energy effect" for *s*-electrons and only the continuum states are influenced by relativistic interactions. The spin-polarization and angular distribution parameters for ionization of the Hg $6s^2$ subshell in the vicinity of the cross section (Cooper) minimum deviate substantially from non-relativistic predictions, as has been experimentally shown recently [46].

In Hg $5d^{10}$ subshell photoionization between thresholds and $h\nu = 40$ eV, the influence of many-electron correlations is quantitatively more important than the small relativistic splitting mentioned. This can be seen by comparing the uncorrelated *DS* calculation for ξ in Figs. 2 and 3 with the correlated RPA calculations and with the experimental results. Similarly, it is visible in the β parameter when the uncorrelated *DS* calculations of Fig. 8 or the DF curves of Figs. 9 and 10 are compared with the correlated theories and the experimental data. For the heavy element Hg, even the non-relativistic but correlated RPAE result of Figs. 4 and 6 agrees very well with the experiments.*

For ξ and β the relativistic and correlated RRPA theory yields the best theoretical results. For the absolute cross sections the same calculation [12] does not show very good agreement with experiment, but more experimental data are needed. Further theoretical investigations of core relaxation effects should bring the theoretical threshold positions closer to the experimental ones, thus improving the overall agreement. The influence of the more tightly bound electrons (e.g. $5p^6$) on the outer shells is still an open question; and also the investigation of two-electron excitations, neglected in all the theories mentioned, requires more experimental and theoretical work.

We would like to express our thanks to F. Combet Farnoux, N. Cherepkov, W. Johnson and S. Manson for useful correspondence as well as for the communication of unpublished results. This work was supported by the DFG and BMFT. One of us (G.S.) wishes to thank the Studienstiftung des Deutschen Volkes for financial support.

References

1. Manson, S.T.: Phys. Rev. Lett. **26**, 219 (1971)
2. Manson, S.T.: Chem. Phys. Lett. **19**, 76 (1973)
3. Cooper, J., Zare, R.N.: J. Chem. Phys. **48**, 942 (1968)
4. Walker, T.E.H., Berkowitz, J., Dehmer, J.L., Waber, J.I.: Phys. Rev. Lett. **31**, 678 (1973) and Berkowitz, J.: Photoabsorption, Photoionization and Photoelectron Spectroscopy New York, San Francisco, London: Academic press 1979
5. Walker, T.E.H., Waber, J.T.: J. Phys. B **7**, 674 (1974)
6. Kim, Y.S., Pratt, R.H., Ron, A., Tseng, H.K.: Phys. Rev. A **22**, 567 (1980)
7. Keller, F., Combet Farnoux, F.: Private communication (May 1981)
8. Tambe, B.R., Ong, W., Manson, S.T.: Phys. Rev. A **23**, 799 (1981)
9. Tambe, B.R., Ong, W., Manson, S.T.: Private communication (July 1980)
10. Ivanov, V.K., Medvedev, S.Yu., Sosnivker, V.A.: Preprint No. 615 of A.F. Joffe Physical-Technical Institute, Leningrad (1979)
11. Cherepkov, N.A.: Private communication (January 1981)
12. Johnson, W.R., Radojević, V., Deshmukh, P., Cheng, K.T.: Private communication (May 1981) and to be published
13. Beutler, H.: Z. Phys. **86**, 710 (1933)
14. Berkowitz, J., Lifshitz, C.: J. Phys. B **1**, 438 (1968)
15. Lincke, R., Stredele, B.: Z. Phys. **238**, 164 (1970)
16. Brehm, B.: Z. Naturforsch. **21a**, 196 (1966)
17. Cairns, R.B., Harrison, H., Schoen, R.J.: J. Chem. Phys. **53**, 96 (1970)
18. Dehmer, J.L., Berkowitz, J.: Phys. Rev. A **10**, 484 (1974)
19. Süzer, S., Hilton, P.R., Hush, N.S., Nordholm, S.: J. Electron Spectrosc. Relat. Phenom. **12**, 357 (1977)
20. Svensson, S., Martensson, N., Brasilier, E., Malmqvist, P.A., Gelius, U., Siegbahn, K.: J. Electron Spectrosc. Relat. Phenom. **9**, 51 (1976)
21. Nilsson, R., Nyholm, R., Berndtsson, A., Hedman, J., Nordling, C.: J. Electron Spectrosc. Relat. Phenom. **9**, 337 (1976)
22. Shannon, S.P., Codling, K.: J. Phys. B **11**, 1193 (1978)
23. Brehm, B., Höfler, K.: Phys. Lett. **68** A, 437 (1978)
24. Harrison, H.: Bull. Am. Phys. Soc. **15**, 1514 (1970)
25. Niehaus, A., Ruf, M.W.: Z. Phys. **252**, 84 (1972)
26. Schönhense, G.: J. Phys. B **14**, L187 (1981)
27. Schäfers, F., Schönhense, G., Heinzmann, U.: Z. Physik, this volume
28. Cherepkov, N.A.: Sov. Phys. JETP **38**, 463 (1974)
29. Lee, C.M.: Phys. Rev. A **10**, 1598 (1974)
30. Kessler, J.: Polarized Electrons. Berlin, Heidelberg, New York: Springer 1976
31. Heinzmann, U., Schönhense, G.: Proc. 6th Internat. Conf. on VUV Radiation Physics, Charlottesville Vol. 3 Abstracts p. 64 (1980) and Schönhense, G.: Diploma Thesis, University of Münster (1978)
32. Schönhense, G.: PhD-Thesis, University of Münster (1981)
33. Brandt, D.: Diploma Thesis, University of Münster (1975)
34. Risley, J.S.: Rev. Sci. Instrum. **43**, 95 (1972)
35. Jost, K., Kessler, J.: Z. Phys. **195**, 1 (1966)
36. Heinzmann, U.: J. Phys. B **11**, 399 (1978)
37. Eitel, W., Jost, K., Kessler, J.: Z. Phys. **209**, 348 (1968)
38. Jost, K., Ohnemus, B.: Phys. Rev. A **19**, 641 (1979)
39. Samson, J.A.R.: Techniques of Vacuum Ultraviolet Spectroscopy. New York: John Wiley (1967)
40. Moore, C.E.: Atomic Energy Levels, NBS Circ. No. 467, Washington (1962)
41. Cherepkov, N.A.: J. Phys. B **13**, L689 (1980)
42. Heinzmann, U., Schönhense, G., Kessler, J.: Phys. Rev. Lett. **42**, 1603 (1979) and J. Phys. B **13**, L153 (1980)
43. Huang, K.-N., Johnson, W.R., Cheng, K.T.: Phys. Rev. Lett. **43**, 1658 (1979)
44. Mansfield, M.W.D.: Astrophys. J. **180**, 1011 (1973)
45. Carter, S.L., Kelly, H.P.: J. Phys. B **11**, 2467 (1978)
46. Schönhense, G., Heinzmann, U., Kessler, J., Cherepkov, N.A.: (to be published)

G. Schönhense
F. Schäfers
U. Heinzmann
Fritz-Haber-Institut der
Max-Planck-Gesellschaft
Faradayweg 4–6
D-1000 Berlin 33
Germany

J. Kessler
Physikalisches Institut der Universität Münster
Domagkstraße
D-4400 Münster
Federal Republic of Germany

* This is mainly because the RPAE phase-shift difference between the εp and εf continuum waves shows excellent agreement with the corresponding phase-shift difference extracted from the experiments [32]